Ann. Geophys., 27, 913–921, 2009
www.ann-geophys.net/27/913/2009/
© Author(s) 2009. This work is distributed under
the Creative Commons Attribution 3.0 License.

Annales Geophysicae

# Remote sensing of local structure of the quasi-perpendicular Earth's bow shock by using field-aligned beams

**B. Miao**[1], **H. Kucharek**[1], **E. Möbius**[1], **C. Mouikis**[1], **H. Matsui**[1], **Y. C.-M. Liu**[1], **and E. A. Lucek**[2]

[1]Dept. of Physics and Institute for the Study of Earth, Oceans and Space, University of New Hampshire, Durham, NH, USA
[2]Space and Atmospheric Physics, Imperial College, London, SW7 2BZ, UK

Received: 7 May 2008 – Revised: 28 January 2009 – Accepted: 28 January 2009 – Published: 2 March 2009

**Abstract.** Field-aligned ion beams (FABs) originate at the quasi-perpendicular Earth's bow shock and constitute an important ion population in the foreshock region. The bulk velocity of these FABs depends significantly on the shock normal angle, which is the angle between shock normal and upstream interplanetary magnetic field (IMF). This dependency may therefore be taken as an indicator of the local structure of the shock. Applying the direct reflection model to Cluster measurements, we have developed a method that uses proton FABs in the foreshock region for remote sensing of the local shock structure. The comparison of the model results with the multi-spacecraft observations of FAB events shows very good agreement in terms of wave amplitude and frequency of surface waves at the shock front.

**Keywords.** Interplanetary physics (Planetary bow shocks; Solar wind plasma) – Space plasma physics (Waves and instabilities)

## 1 Introduction

The global shape of Earth's bow shock is well known and can be modeled by using a magnetohydrodynamics approach. However, the details of the local structure of the bow shock are still not very well understood. The various shock regions are commonly distinguished by the shock normal angle ($\theta_{Bn}$), which is the angle between the upstream IMF and the normal ($\boldsymbol{n}$) to the shock front. Angles of $\theta_{Bn} \leq 45°$ correspond to the quasi-parallel regime whereas angles of $\theta_{Bn} \geq 45°$ are corresponding to quasi-perpendicular shock regions, respectively. Both the shock structure and presence of ion population are quite different at those two distinct regions. The overall structure of the quasi-perpendicular Earth's bow shock is controlled by the reflected ion population, the gyrating population at the shock ramp and the dynamics of the incoming solar wind.

FABs are a prominent feature upstream of the (quasi-) perpendicular regime of the bow shock and, typically, the energy of FABs is above 10 keV and can be up to 30 keV or more (e.g. Asbridge et al., 1968; Lin et al., 1974; Bale et al., 2005). However, there are a number of open questions concerning ion reflection as well as ion beam formation at quasi-perpendicular shocks (e.g. Gosling et al., 1978; Möbius et al., 2001; Kucharek et al., 2004). The ion reflection and the formation of these beams might be controlled by a number of parameters, including $\theta_{Bn}$, Mach number ($M_A$), solar wind velocity ($\boldsymbol{V}_{sw}$) and the angle between $\boldsymbol{V}_{sw}$ and $\boldsymbol{n}$ ($\theta_{Vn}$).

Large scale waves along the flanks of the bow shock can be caused by variations in the dynamic pressure of the solar wind. Small and medium scale waves such as the shock ripples are created by instabilities inside the shock ramp. All large, medium, and small scale waves may lead to variations of the local shock normal angle. In this investigation we will concentrate on the small scale structures determined by the local shock structure. In general the local shock structure, such as ramp, foot and overshoot, are related to behavior of gyrating ions (Horbury et al., 2002; Bale et al., 2003). Numerical simulations, using hybrid and full particle codes, have predicted shock front instabilities which may lead to so-called shock ripples (Lowe and Burgess, 2003; Burgess and Scholer, 2007). Most recently observational evidence for these ripples has been provided by Moullard et al. (2006). Those authors found that these ripples are propagating along the shock surface and roughly in the direction of the magnetic field. The phase speed of the ripples is 2 to 4 times the Alfvén velocity ($v_A$), i.e. 80–160 km s$^{-1}$, and the wavelength is approximately 15 to 30 times the upstream ion initial length ($c/\omega_{pi}$), which corresponds to 1000–2000 km.

According to ISEE observations, Paschmann et al. (1980) showed that the ratio $E_r/E_i$ (energy of the reflected beams

*Correspondence to:* B. Miao
(bmiao@unh.edu)

Published by Copernicus Publications on behalf of the European Geosciences Union.

$E_r$ over the incoming solar wind energy $E_i$) agrees well with the results predicted by a direct reflection model (Sonnerup, 1969), assuming conservation of the ion magnetic moment. Based on this conservation, the relationship between the FABs velocity $\boldsymbol{V}_b$, $\boldsymbol{V}_{sw}$, $\boldsymbol{n}$, $\theta_{Bn}$ and $\theta_{Vn}$ is determined. By studying the distribution functions of FABs, the variations in the FABs velocity and intensity are observed. These variations may result from upstream IMF variations, solar wind turbulence, Alfvén waves and the resulting changes in the local shock structure. If these effects can be separated in case studies, a unique relationship between FABs and the local shock structure may be applied to remotely sense the local shock surface. This kind of approach is of significant importance for shocks which are not easily accessible (for instance the termination shock) because spacecraft do not have to cross the shock to obtain information about the local shock structure.

The primary goal of this paper is to provide a basic method, which allows inferring the local structure of the shock by observing the velocity variations of FABs. The paper is organized as follows. In the second section we describe the model. In the third section we introduce the observation used in this study and the corresponding data analysis. The results of numerical study and model predictions are discussed in the fourth section of this paper. Finally, we will summarize the results of this investigation.

## 2 Method

### 2.1 Determine the shock normal *n*

Figure 1 is a sketch that shows the basic points of the remote sensing local structure of the shock front. As shown in Fig. 1, a part of the incoming solar wind ions are reflected at the shock front to travel along the magnetic field line, which has a convection velocity ($\boldsymbol{V}_{sw}$) towards the downstream of bow shock. The velocity and intensity of those reflected ion beams (FABs) are affected by the geometry of shock front. The variation of FABs' velocity may indicate the uneven shock surface. Thus, the local structure of bow shock can be estimated by using the geometry relationship between the observed FABs' velocity, velocity of solar wind and magnetic field.

The reflected FABs are recognized as a fraction of reflected solar wind ions, which are accelerated by the motional electric field at the bow shock. The velocity of FABs are well explained by the direct reflection model introduced by Sonnerup (1969), which is also called as $\mu$ conserving reflection by Schwartz et al. (1983) due to the conservation of ions' magnetic moments $\mu_m$. In the direct reflection model, a simple geometrical relationship between shock normal $\boldsymbol{n}$, upstream IMF $\boldsymbol{B}$, incoming solar wind velocity $\boldsymbol{V}_{sw}$ and FABs velocity $\boldsymbol{V}_b$ is defined. It is convenient to describe the direct reflection model in the de Hoffman-Teller (HT) frame (de Hoffman and Teller, 1950), which is a moving frame to cancel out the motional electric field at the bow shock. Accordingly, the direct reflection model shows the conservation of kinetic energy of incoming and reflecting ions flow in the HT frame.

The following equation is the definition of the HT velocity:

$$\boldsymbol{V}_{HT} = \frac{\boldsymbol{n} \times (\boldsymbol{V}_{sw} \times \boldsymbol{B})}{\boldsymbol{B} \cdot \boldsymbol{n}}, \tag{1}$$

which is equivalent to the following equation (Schwartz and Burgess, 1984):

$$\frac{V_b{}'}{V_{sw}{}'} = \frac{\cos\theta_{Bn}}{\cos\theta_{Vn}}\left(\cos\theta_{BV} + \sqrt{\frac{V_b^2}{V_{sw}^2} - \sin^2\theta_{BV}}\right) - 1. \tag{2}$$

$V_b{}'$ and $V_{sw}{}'$ are velocities of FABs and solar wind in the HT frame; $V_b$ and $V_{sw}$ are velocities of FABs and solar wind in the spacecraft frame, respectively. $\theta_{BV}$ is the acute angle between $\boldsymbol{B}$ and $\boldsymbol{V}_{sw}$.

The assumption of energy conservation of ion flow requires the left hand side of the Eq. (2) is equal to 1.

$$\frac{V_b{}'}{V_{sw}{}'} = 1 \tag{3}$$

The each component of vector Eq. (1) can be written as one set of homogenous linear equations about shock normal $\boldsymbol{n}$. Unfortunately, the rank of the coefficients matrix is 1, so that the $\boldsymbol{n}$ cannot be determined uniquely. Thus, the additional constraints of $\boldsymbol{n}$ are necessary to be introduced as follows:

1. $\boldsymbol{n}$ is always pointing to the upstream from the downstream of bow shock;
2. $\boldsymbol{n}$ is first assumed in the $\boldsymbol{V}_{sw}$–$\boldsymbol{B}$ plane; subsequently, we allow $\boldsymbol{n}$ is out of the $\boldsymbol{V}_{sw}$–$\boldsymbol{B}$ plane with some certain angle as shown in Fig. 2b.

The $\boldsymbol{B}$, $\boldsymbol{V}_b$ and $\boldsymbol{V}_{sw}$ in Eq. (2) are all obtained by the observation. Thus, Eqs. (2), (3) and additional constraints can be used to calculate the $\boldsymbol{n}$ uniquely.

### 2.2 Motion of the average shock front

In order to determine the uneven shock surface, we need to trace the FABs to their origin at the shock front and then calculate shock normal vectors on the shock front. Tracing the FABs to the shock front requires the location and motion of the average shock front. Using timing analysis method (e.g. Russell et al., 1983; Harvey, 1998; Schwartz, 1998), the shock normal vectors and shock speeds are determined at inbound or outbound shock crossing events. Based on the velocities of the shock front at crossing events, the motion of the average shock front (the black horizontal straight line in Fig. 1) between the two crossings is deduced. The shock velocity at the first crossing is as the initial velocity ($\boldsymbol{v}_i$) and the shock velocity at the second crossing is as the final velocity

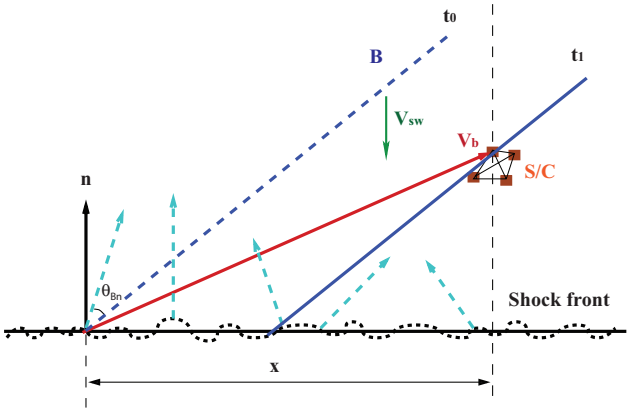


**Fig. 1.** The black horizontal straight line is the average shock front and the vertical black arrow is the shock normal ***n***; the black dashed curve is the possible shock structure and the light blue arrows are the local shock normal vectors (not to scale); The red arrow is the velocity of FABs; The blue dashed and solid lines are IMF at different time which is moving with $\boldsymbol{V}_{sw}$; The beam is located at the shock at $t_0$, while arriving at the location of SC3 at $t_1$; x is the projection of the FABs traveling path along the shock front.

($\boldsymbol{v}_f$). If the $\boldsymbol{v}_i$ and $\boldsymbol{v}_f$ are approximately along a straight line (shown as a vertical dashed line in Fig. 1), the motion of the shock can be simplified to a 1-D motion (The details will be described in Sect. 3). After the shock normal vectors are located (i.e. the x in Fig. 1 is determined), we may describe the local structure of shock front, accordingly.

### 2.3 Use surface waves to describe the local structure

Hybrid simulations are used to find the properties of the surface waves we are most likely seeing at those shock crossings. In a recent paper (Burgess and Scholer, 2007), authors pointed out that the gyrating ion population at the shock front is closely associated with the waves at the shock ramp. We used the results of this paper to obtain limits for the wavelength and amplitude for our model described below.

In our current model we introduce two surface waves, perpendicular to each other, which are preestablished at the average shock front (so called forward model), as shown in Fig. 2a. Those two surface waves are marked as $\boldsymbol{k}_1$ and $\boldsymbol{k}_2$. The wave $\boldsymbol{k}_1$ is roughly along the projection of upstream IMF ***B***.

The goal of our numerical approach is using the direct reflection model and reproducing the observed bulk beams speed variations by introducing sinusoidal waves, which simulates the local shock structure. In an iterative process wavelength and amplitude are updated to obtain the best fit to the observed time series of the FABs speeds.

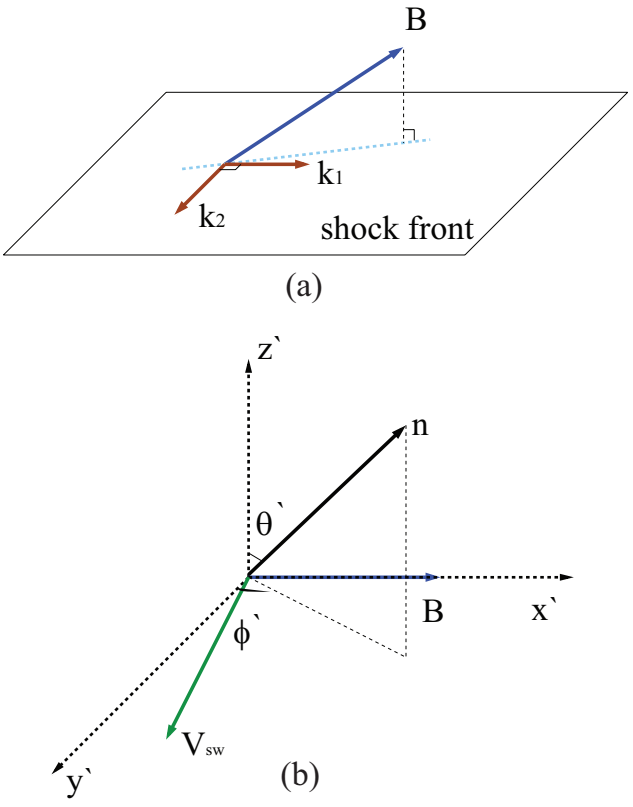


**Fig. 2.** **(a)** 2-D plane surface waves are added to the shock front to reproduce the measured FABs; the projection of the ***B*** is set as a referred direction; Plane waves $\boldsymbol{k}_1$ and $\boldsymbol{k}_2$ are perpendicular to each other. **(b)** shows the correspondent coordinate system where the shock normal vector ***n*** is out of the $\boldsymbol{B}$–$\boldsymbol{V}_{sw}$ plane.

## 3 Data

For this study observational data are provided by the Cluster spacecraft. We use the fluxgate magnetometer (FGM) to obtain high time resolution (about 22 measurements per second) magnetic field data (Balogh et al., 2001); and the composition and distribution function analyzer (CODIF) to obtain the proton's distribution function in velocity space. The solar wind bulk velocity is derived from hot ion analyzer (HIA) (Rème et al., 2001). Both CODIF and HIA sensors are called CIS (Cluster Ion Spectrometry) instruments.

For the present study we identified the following shock crossing events: on 7 April 2001, 20:17:00–20:23:00 UTC, on 29 December 2003, 05:41:00–05:46:00 UTC, on 14 January 2004, 08:12:00–08:15:00 UTC and on 3 April 2004, 20:51:00–21:06:00 UTC which will be discussed in detail. During these time periods, the separation of the Cluster spacecraft was between 400 and 1000 km.

Figure 3 shows an outbound and an inbound crossing on 7 April 2001, 20:17:00 and 20:23:00 UTC. From top to bottom the figure shows energy spectrum, ion density, solar wind

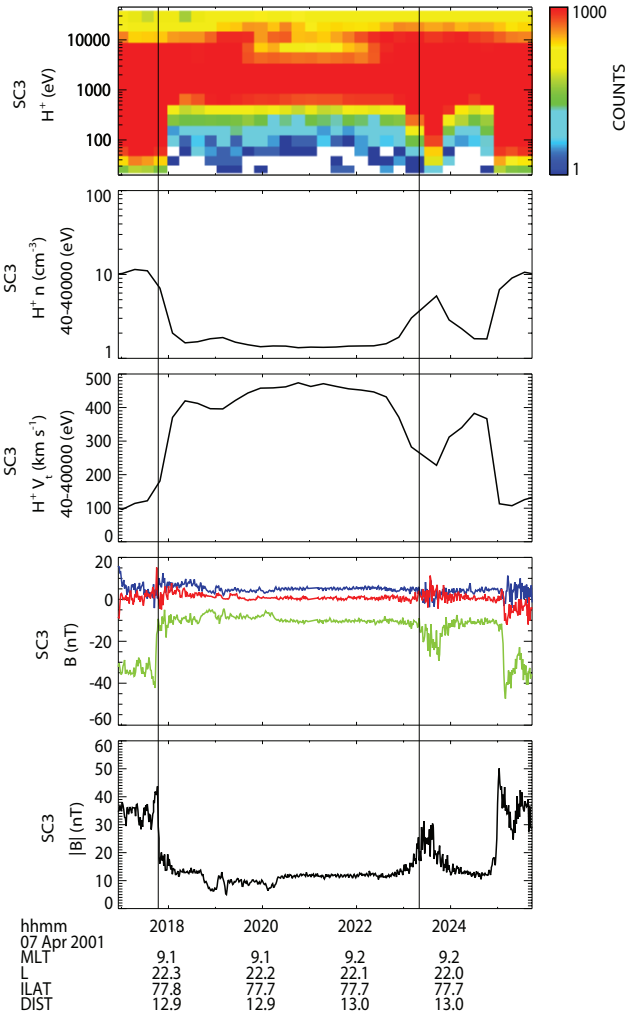


**Fig. 3.** The top panel is proton's energy spectrum according to Cluster SC3 CODIF's data. The remaining panels are number density of protons, bulk velocity of protons, $\boldsymbol{B}$ and magnitude of B . The two vertical lines mark the positions of shock crossing events.

bulk speeds, each component of the magnetic field and its magnitude as a function of time from spacecraft 3 (SC3). Vertical lines mark the outbound and the inbound crossings, respectively. Clearly, the sudden changes in the solar wind speeds, density, and magnetic field can be identified. Upstream of the shock, in the solar wind, we observe a high energy populations at ∼10 keV (the field-aligned ion beams as we will discuss later).

### 3.1 Average shock normal and shock speeds

In order to trace the FABs to the shock front, the location of the shock front is required. To determine the actual shock position we take advantage of Cluster as a multi-spacecraft mission and we perform a timing analysis between two consecutive shock crossings. Using $\boldsymbol{v}_i$, $\boldsymbol{v}_f$, initial displacement, $\boldsymbol{s}_i$, and final displacement, $\boldsymbol{s}_f$, the displacement of shock front can be simplified as a three-order polynomial function of time (Haaland et al., 2004), i.e.:

$$s(t) = a_0 + a_1 t + a_2 t^2 + a_3 t^3, \tag{4}$$

and then the velocity of shock front is:

$$v(t) = a_1 + 2a_2 t + 3a_3 t^2. \tag{5}$$

For our investigations we have chosen two adjacent shock crossings. Timing analysis method has been used to determine the shock normal of $\boldsymbol{n}_i$ = (0.91, −0.12, 0.18) and shock speed of $v_i$=14 km s$^{-1}$ at outbound crossing, left side of Fig. 3; At inbound crossing, right side of Fig. 3, shock normal $\boldsymbol{n}_f$=(0.95, −0.18, 0.27) and shock speed of $v_f$=5 km s$^{-1}$. The time span between the shock crossings is of the order of 6 min. As one can see, the two shock normal vectors $\boldsymbol{n}_i$ and $\boldsymbol{n}_f$ are nearly the same, with difference of about 5.5°. Thus, we assume that, between the two crossing events, the shock front is moving with a non-constant acceleration in one dimension. This allows us to determine the distance to the shock front by solving the equations of motion.

### 3.2 Observation of field-aligned beams

For this study a number of shock crossings have been investigated. In the top panel of Fig. 3, a beam like feature can be identified in the energy spectrum at around 10 keV. The proton phase space distribution clearly shows that FABs are present. The best time resolution of CIS instrument is one spin period, i.e. 4 s. For our case study, distribution functions are accumulated for all 16 energy levels in the energy range from 10 to 40 keV, over 16 s. The top panel of Fig. 4 shows a time series of distribution functions in the velocity space; the bottom panel of Fig. 4 shows 1-D cuts through the center of the FABs, along the $V_{\text{para}}$ (green line) and $V_{\text{perp}}$ (black line) directions, respectively. In the figure, $V_{\text{para}}$ is the velocity parallel to the IMF $\boldsymbol{B}$ whereas $V_{\text{perp}}$ denotes the component that is perpendicular to the magnetic field. The yellow pattern, with $V_{\text{para}}$=−450 km s$^{-1}$ at the core, is the solar wind distribution and the light blue pattern, with $V_{\text{para}}$=1200 km s$^{-1}$ at the core, is FABs distribution, which has inverse sign of $V_{\text{para}}$ and similar $V_{\text{perp}}$ while comparing to the bulk velocity of the solar wind. The magnitude of the FABs velocity is given by $V_b = \sqrt{V_{\text{para}}^2 + V_{\text{perp}}^2}$. The beams can be observed during most of the time period when the spacecraft is upstream of the bow shock. During this time period the peak of the beams distribution (located at the crossing of dashed lines) is changing its location in velocity space. These temporal evolutions may be due to wave forms or structures at the shock ramp. This is the subject of the next section in which we will use our numerical model to infer information on the local shock structure.

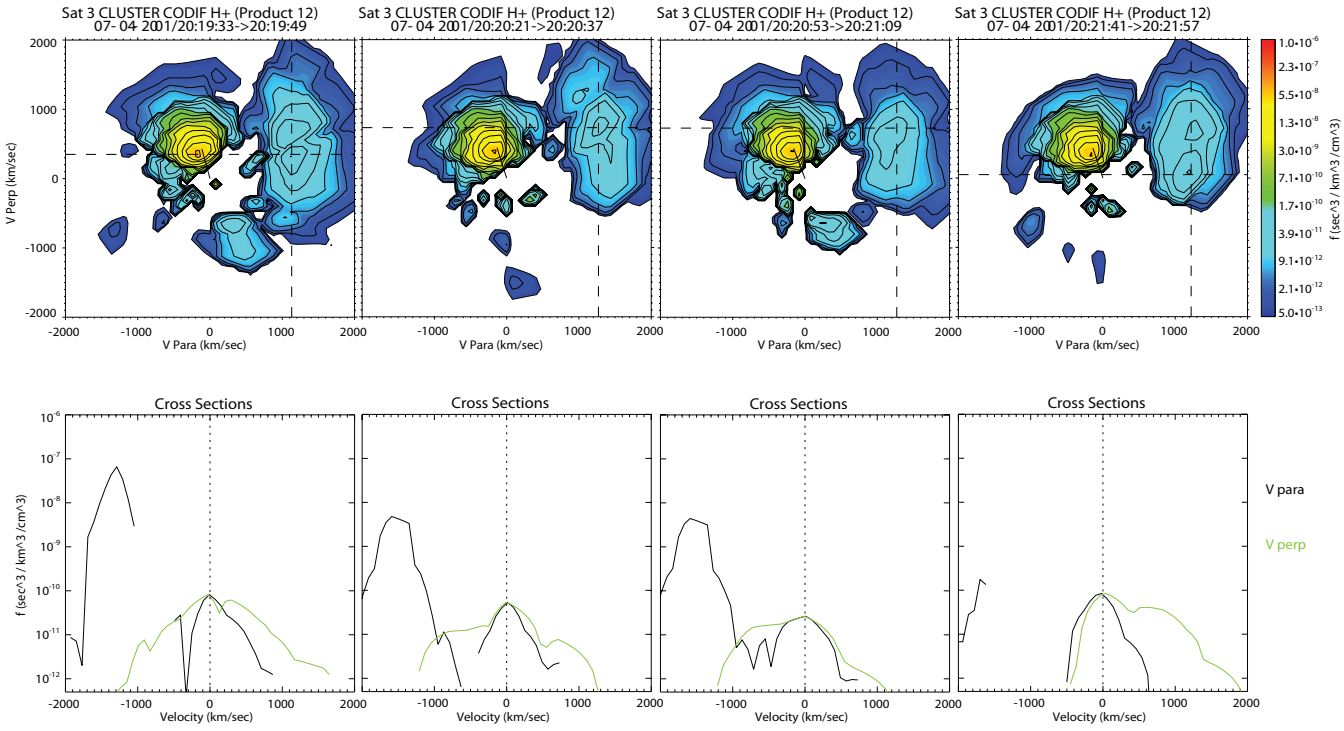


**Fig. 4.** Proton's distribution functions in the velocity space are shown in the spacecraft frame. The V-para axis is along direction of IMF measured by Cluster's FGM instrument and the V-perp axis is a direction normal to IMF. From the left panel to right panel are distribution functions on 7 April 2001 at 20:19:33–20:19:49 UTC, 20:20:21–20:20:37 UTC, 20:20:53–20:21:05 UTC and 20:21:41–20:21:57 UTC. Top panel shows the 2-D distribution function, while the bottom panel shows a cut along the distributions function indicated by the dashed lines.

## 4 Results from our numerical study

In this section we will now apply our numerical model which has been introduced in Sect. 2. As described above we will iteratively vary the wave number and the wave amplitude of the introduced plane waves which are supposed to mimic the local shock structure. For our case studies, the FABs velocity and calculated $\theta_{Bn}$ are reproduced by superimposing 2-D surface plane waves onto the average shock surface.

In Fig. 5 we show four selected shock crossings at which Cluster SC1 or SC3 observes FABs. SC1 observes these beams on 3 April 2004 at 20:51:00–21:06:00 UTC, whereas SC3 observes other events on 7 April 2001 at 20:17:00–20:23:00 UTC, on 29 December 2003 at 05:41:00–05:46:00 UTC and on 14 January 2004 at 08:12:00–08:15:00 UTC. From top to bottom this figure shows the distance of the spacecraft to the shock front determined by timing analysis, the beams bulk speeds and the shock normal angles determined by the models. In the middle panels of Fig. 5a, b and c the observed velocities of FABs are well reproduced. The red lines show the observed FABs speeds; the blue lines represent the calculated FABs speeds. As one can see, the numerical models reproduce the observed beams' bulk speeds very well. In the bottom panel we show $\theta_{Bn}$ determined by the various methods. The blue lines show the $\theta_{Bn}$ calculated with the preestablished local structure (sine wave) according to the forward model; the green lines show the $\theta_{Bn}$ calculated with Eqs. (2), (3) and constraint that $\boldsymbol{n}$ is out of $\boldsymbol{B}$–$\boldsymbol{V}_{sw}$ plane with the selected angle; the red lines show the $\theta_{Bn}$ calculated with the similar way as green lines but $\boldsymbol{n}$ is within the $\boldsymbol{B}$–$\boldsymbol{V}_{sw}$ plane. The green lines are perfectly matched with the blue lines. Due to the lack of match between blue and red lines, the $\boldsymbol{n}$, $\boldsymbol{B}$ and $\boldsymbol{V}_{sw}$ coplanar model cannot reproduce the $\theta_{Bn}$. Schwartz and Burgess (1984) also mentioned that "the direction of $\boldsymbol{n}$ does not, in general, lie in the $\boldsymbol{B}$–$\boldsymbol{V}_{sw}$ plane". These results are obtained for the parameters listed in Table 1 (first 3 rows).

The local structure may be approximately described by those 2-D surface plane waves. The surface plane wave by using subscript 1 ($\lambda_1$, $A_1$, $V_{\text{phase1}}$), is corresponding to the B-in-plane-wave according to the 2-D hybrid simulation work (Burgess and Scholer, 2007); The surface plane wave by using subscript 2 ($\lambda_2$, $A_2$, $V_{\text{phase2}}$), is corresponding to the B-out-of-plane-wave. From Table 1, the B-in-plane-wave has long wavelength and small amplitude which is interpreted as an ultra-low frequency surface wave. The variation of FABs velocity is mainly affected by the B-out-of-plane-wave, wave $\boldsymbol{k}_2$.

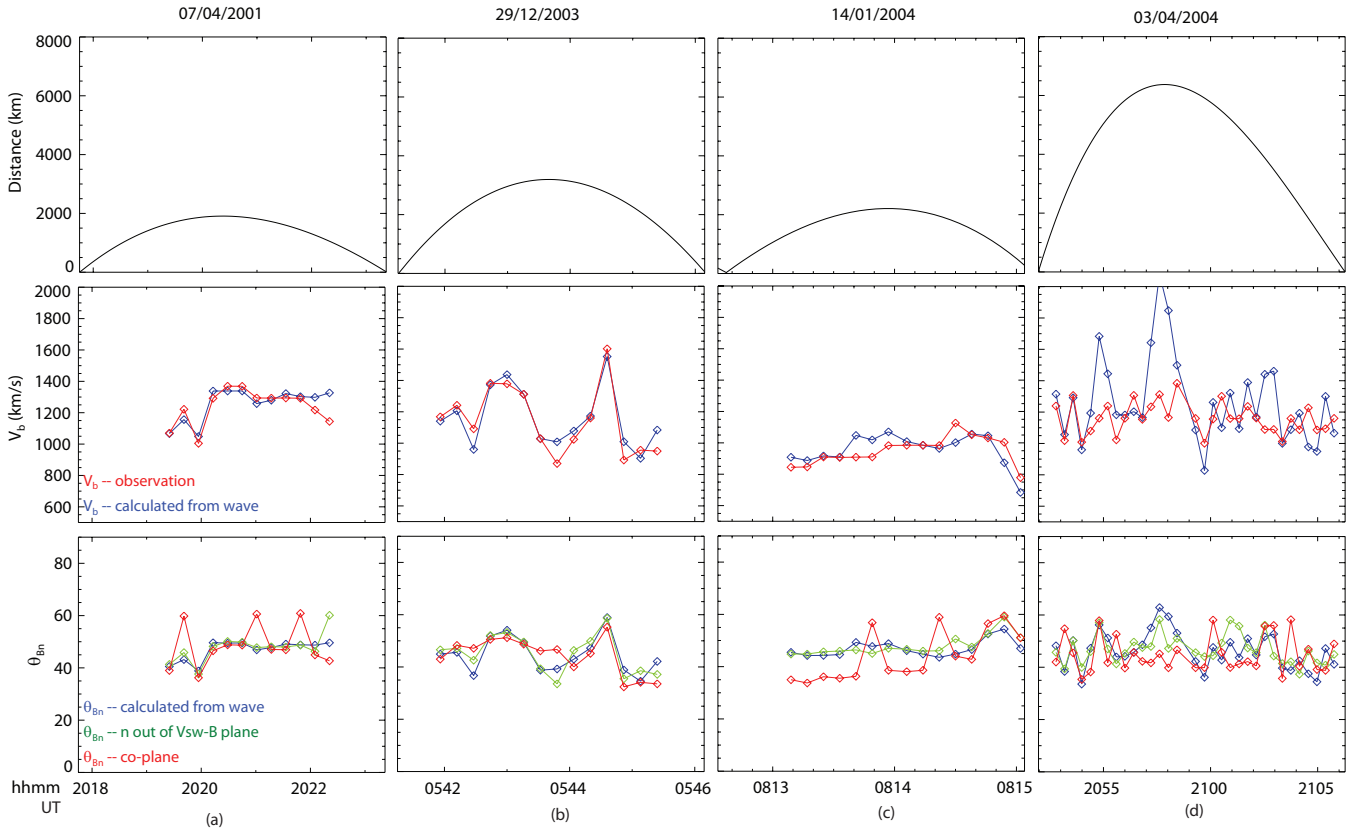


**Fig. 5.** The top panels for the distance from the SC3 to the average shock front; the middle panels for the speed variations of the observed FABs (red line) and the calculated FABs (blue line) according to the forward model; the bottom panels for the $\theta_{Bn}$ and the blue line for the forward model, the green line for the $\boldsymbol{n}$ out of $\boldsymbol{B}$–$\boldsymbol{V}_{sw}$ plane analytic method, the red line for the $\boldsymbol{n}$, $\boldsymbol{B}$ and $\boldsymbol{V}_{sw}$ coplanar.

For the 7 April 2001 case, the angle of $\boldsymbol{n}$ out of the $\boldsymbol{B}$–$\boldsymbol{V}_{sw}$ plane is 15°; For the 29 December 2003 case, the $\boldsymbol{n}$ is 20° out of the plane; For the 14 January 2004 case, the $\boldsymbol{n}$ is 30° out of the plane. The matched shock normal angles $\theta_{Bn}$ indicate the shock normal vectors $\boldsymbol{n}$ are limited in a plane. This means that the 1-D surface wave (limited in our case studies) mainly controls the local structure of shock front. The different angles of $\boldsymbol{n}$ out of the plane indicate the contribution of surface wave $\boldsymbol{k}_1$ to the local structure of the shock front.

In error analysis, the standard deviation of upstream $\boldsymbol{V}_{sw}$ and high time resolution $\boldsymbol{B}$ can be obtained from the level 2 data of Cluster. Due to the middle panels of Fig. 5, the deviation between the observed $V_b$ and the calculated $V_b$ from wave is approximately recognized as the deviation of $V_b$. Applying error propagation, we performed an error estimate (Bevington et al., 2003) for $\theta_{Bn}$ that is calculated from wave (blue line) in the case study for 7 April 2001, in which we obtained $\triangle\theta_{Bn}$=±3°.

All three case studies (a, b and c) are in a relatively short time period, 3–5 min, and the 1-D surface wave $\boldsymbol{k}_2$ is the major wave to describe the local structure perfectly. However, for the case study for 3 April 2004 (Fig. 5d), the time period is relatively longer, 10–15 min, and then the mono-frequency 1-D surface wave is no longer suitable to describe the local structure. The middle panel of Fig. 5d shows that the mono-frequency surface wave cannot reproduce the observed FABs speeds; the bottom panel of Fig. 5d also shows that the constraint ($\boldsymbol{n}$ out of plane with one certain angle) is not applicable, in this case study, to reproduce the $\theta_{Bn}$. This might have several reasons. First, the local structure of the shock front is actually 3-D and consists of several wave modes. Second, distance to the shock front is too large and we sample over a large area range of the shock surface so that we might see several different areas which may have different reflection properties. One possible way to investigate those effects might be to introduce multi-dimensional multi-frequency surface waves. Since, the scope of this paper is to present the basic concept idea of remote sensing we treat these more complicated cases as a subject for future investigations.

**Table 1.** Plasmas and wave parameters: comparison of 4 case studies 2-D surface plane waves, direct observation and 2-D hybrid simulation results.

| | Case 7 Apr 2001 | Case 29 Dec 2003 | Case 14 Jan 2004 | Case 3 Apr 2004 | Direct observation | 2-D hybrid (B-in-plane) | 2-D hybrid (B-out-of-plane) |
|---|---|---|---|---|---|---|---|
| $\theta_{Bn}$ | ∼50° | ∼45° | ∼50° | ∼50° | 87° | 88° | 90° |
| $M_A$ | 5.7 | 5.2 | 2.6 | 6.2 | 11.4 | 5.7 | 7.2 |
| $V_{sw}/v_i$ ($v_A$) | 6.2 | 6.4 | 3.6 | 7.3 | 14.9 | 4 | 5 |
| $\lambda_1$ (c/$\omega_{pi}$) | 27.8 | 25.0 | 21.8 | 51.1 | 15–30 | 4–8 | – |
| $A_1$ (c/$\omega_{pi}$) | 0.7 | 0.5 | 0.5 | 1.0 | | ∼1.0 | – |
| $V_{\text{phase1}}$ ($v_A$) | 31.0 | 8.0 | 35.2 | 30.1 | 2–4 | – | – |
| $\lambda_2$ (c/$\omega_{pi}$) | 6.2 | 6.2 | 4.9 | 11.7 | – | – | 7.5 |
| $A_2$ (c/$\omega_{pi}$) | 0.7 | 0.7 | 1.3 | 1.0 | – | – | ∼1.0 |
| $V_{\text{phase2}}$ ($v_A$) | 7.9 | 0.0 | 0.0 | 0.0 | – | – | 7.5 |

## 5 Discussion

From those case studies presented above we infer amplitudes, wavelengths and phase speeds of the local shock structure at the shock ramp on 7 April 2001, 29 December 2003 and 14 January 2004 (Table 1, last 6 rows). For the 7 April 2001 case, amplitude $A$=50 km, wavelength $\lambda$=440 km and $\omega$=8.0 $\omega_{ci}$. The wave parameters are normalized by upstream ion initial length (c/$\omega_{pi}$∼71 km) or Alfvén velocity ($v_A$∼82 km s$^{-1}$) as follows: $\lambda=2\pi/k$=6.2 c/$\omega_{pi}$, $A$=0.7 c/$\omega_{pi}$ and $v_{\text{phase}}$=7.9 $v_A$. These plasma parameters are based on average value of $\theta_{Bn}$=55° to 60°, Alfvén Mach number $M_A$=5.3 and $V_{sw}$=530 km s$^{-1}$.

In the 2-D hybrid simulation of Lowe and Burgess (2003), the surface waves propagating along the shock have $\lambda$=4 to 8 c/$\omega_{pi}$ when $\theta_{Bn}$=88°, $M_A$=5.7, $\beta_i$=0.5 and $V_{in}$=4$v_A$ ($V_{in}$ is the bulk velocity of incoming ions in the upstream, i.e. solar wind velocity).

In the most recent simulation of Burgess and Scholer (2007), they repeated the 2-D hybrid simulation with $\boldsymbol{B}$ in the simulation plane and obtained a wavelength $\lambda$=6 c/$\omega_{pi}$, $M_A$=5.0 and $\beta_i$=0.5 for the surface waves (ripples). They also reported on simulations of the ripple structures with magnetic field orientations out-of-plane. The ripple wavelength is 7.5 c/$\omega_{pi}$ (as obtained from Fig. 3. in Burgess and Scholer, 2007) for $M_A$=7.6 and $\beta_i$=0.5. This wavelength is longer than the one obtained from the simulation with B-in-plane ($\lambda$=2–5 c/$\omega_{pi}$, $M_A$=7.1 and $\beta_i$=0.5). From Table 1, our results are close to the results of B-out-of-plane hybrid simulation. One difference, however, should be noted that their 2-D hybrid simulation work has $\boldsymbol{B}$ in the simulation plane, i.e. propagating direction $\boldsymbol{k}$ of surface wave, shock normal $\boldsymbol{n}$ and $\boldsymbol{B}$ are co-planar. In our case study the wave vector $\boldsymbol{k}$ is not co-planar with $\boldsymbol{B}$ and $\boldsymbol{n}$. The $\boldsymbol{k}$ is around 30° biased from the direction of projection of upstream **B** instead. The reason for this biased angle is still an open question.

Recent observations of ripples on the quasi-perpendicular shock front by Moullard et al. (2006) have been interpreted as traveling ripples within the thin shock layer with a phase speed of 2 to 4 times $v_A$ (i.e. 80–160 km s$^{-1}$) roughly along $\boldsymbol{B}$, a wavelength of approximately 15 to 30 times c/$\omega_{pi}$, i.e. 1000–2000 km and $M_A$=11.4 (shown Direct observation column of Table 1). Moullard et al. have noted the obvious discrepancy in the ripple wavelength and phase speed between their observations and the 2-D hybrid simulation results. Due to different plasma conditions in Moullard's and our analysis, we cannot compare both observations directly. The differences between the two observations indicate that there may be a variation in wavelength and phase speed for those surface waves in the quasi-perpendicular shock front depending on the plasma conditions.

Another problem on the analysis is the difference of $\theta_{Bn}$ which is obtained by using different method. In Fig. 5, for example, 7 April 2001 case shows that the $\theta_{Bn}$ is about 50°, which is somewhat lower than the average $\theta_{Bn}$ about 55° to 60° given by the timing analysis method. This is due to the pitch angle scattering of FABs (Kucharek et al., 2004), in which the parallel component of $\boldsymbol{V}_b$ is decreasing while the perpendicular component of $\boldsymbol{V}_b$ is increasing. If we use the FABs peak pattern in the distribution function, the measured velocity of FABs would be lower than the theoretical velocity of FABs (without considering scattering effect) predicted by the direct reflection model and $\theta_{Bn}$ (determined by timing analysis method). Thus, underestimated FABs velocity might cause a lower $\theta_{Bn}$.

In our analysis, the spatial resolution of the local shock structure is mainly limited by the time resolution of CODIF data (16 s in our case study). The accuracy in the studies of the shock surface structure using FABs also depends on shock motion, $\theta_{Bn}$, $\theta_{Vn}$, and the solar wind velocity. For example, during 7 April 2001, 20:19:00–20:22:00 UTC, the shock normal angle of average shock front $\theta_{Bn}$ = 55° and average shock speed is 16 km s$^{-1}$. The spatial resolution is mainly determined by the motion of average shock front and shock normal angle. Thus, the FABs distribution function

averaged in 16 s is originated from shock surface with a length of up to hundred kilometers. Because the wavelength of major 1-D surface plane wave is 440 km (7 April 2001 case) according to our analysis, the spatial resolution of our method is high enough to reveal the surface waves in the case study. However, if the average $\theta_{Bn}$ is close to 90°, the resolution would be dramatically lower. The resolution also decreases as well as the shock speed increases.

Our analysis requires high energy and angular resolution of FABs. The CODIF instrument has angular resolution of 11.5° and global data interpolation is necessary to gain the direction of peak distribution of FABs. This is the another source of uncertainty.

According to the numerical simulations (e.g. Lembège and Savoini, 1992; Hada et al., 2003; Scholer et al., 2003), shock self-reformation can lead to variation of the locations of the quasi-perpendicular shock. This process also causes variation of the $\theta_{Bn}$ and this in turn leads to the variation of FABs' velocity and intensity. In this study, we have used sinusoidal waves which are superposed on a planar shock to reproduce the velocity variation of FABs. Good agreement with observation has been achieved. In principal, the range of plasma parameters allows reformation, therefore we cannot exclude self-reformation. The $M_A$ of the selected cases is about 5 (see Table 1) and $\beta_i$ is 0.5 or higher. Shock self-reformation is observed under the cases that have the higher $M_A$ and lower $\beta_i$ (less than 0.4) in the simulations (Lembège and Savoini, 1992). However in the later full particle simulation by Hada et al. (2003), which has larger ion/electron mass ratio (∼84), shows that the self-reformation may occur at relatively low $M_A$ (2–5) and it disappears when $\beta_i$ is high. The average shock normal angles of the cases, 55°–60°, are close to 62° which is the critical angle when self-reformation occurs (Lembège and Savoini, 1992). However, due to the time resolution of the CIS instrument we would not be able to distinguish the effect of shock ripples and shock reformation. Similar discussion on CIS observation and self-reformation can be found in Meziane et al. (2007) and Lobzin et al. (2007). High resolution FGM data might provide more information on distinguishing shock ripples and reformation. However, we consider this as a subject of future investigations.

## 6 Summary

In this paper we have introduced a new technique that allows us to remote sense the local structure of the quasi-perpendicular Earth's bow shock. For this study we have assumed that the variations of the bulk velocity of the FABs are associated with local changes of the shock normal angle caused by surface waves or surface ripples. These assumptions are based on the direct reflection model. The proposed model is an iterative numerical model that allows to introduce 2-D surface waves that simulate the local shock structure. Wavelength and wave amplitudes are variables which are determined by fitting the observed time variations of the FABs. We have introduced a basic approach in which we have limited the shock normal to lie in the plane of the incoming solar wind and the interplanetary magnetic field. In a second approach we even allowed shock normals out of that plane.

The comparison of the obtained wavelength and amplitudes from this model with hybrid simulations showed very good agreement. The limitation of this approach for long time period cases might be solved by introducing multi-frequency and multi-dimension surface waves. It should be noted that the advantage of such approach is that the spacecraft does not have to measure in the shock ramp to provide information of the local shock structure. Shock crossings are usually fast and data are limited. Furthermore, such an approach is not limited to the Earth's bow shock. It can be applied to any other stationary shock which is not so easily accessable such as the termination shock.

*Acknowledgements.* This work was supported by NASA under the grant number NNG04GF23G.

Topical Editor R. Nakamura thanks D. Burgess and another anonymous referee for their help in evaluating this paper.

## References

Asbridge, J. R., Bame, S. J., and Strong, I. B.: Outward flow of protons from the Earth's bow shock, J. Geophys. Res. 73(12), 5777–5782, 1968.

Bale, S. D., Mozer, F. S., and Horbury, T. S.: Density-Transition Scale at Quasiperpendicular Collisionless Shocks, Phys. Rev. Lett., 91, 265004, doi:10.1103/PhysRevLett.91.265004, 2003.

Bale, S. D., Balikhin, M. A., Horbury, T. S., Krasnoselskikh, V. V., Kucharek, H., Möbius, E., Walker, S. N., Balogh, A., Burgess, D., Lembège, B., Lucek, E. A., Scholer, M., Schwartz, S. J., and Thomsen, M. F.: Quasi-perpendicular Shock Structure and Processes, Space Sci. Rev., 118, 1–4, 161, doi:10.1007/s11214-005-3827-0, 2005.

Balogh, A., Carr, C. M., Acuña, M. H., Dunlop, M. W., Beek, T. J., Brown, P., Fornacon, K.-H., Georgescu, E., Glassmeier, K.-H., Harris, J., Musmann, G., Oddy, T., and Schwingenschuh, K.: The Cluster Magnetic Field Investigation: overview of in-flight performance and initial results, Ann. Geophys., 19, 1207–1217, 2001, http://www.ann-geophys.net/19/1207/2001/.

Bevington, P., Robinson, D., Bruflodt, D., and Cotkin, S. (Eds.): Data Reduction and Error Analysis, McGraw-Hill, Kent A. Peterson, USA, 2003.

Burgess, D. and Scholer, M.: Shock front instability associated with reflected ions at the perpendicular shock, Phys. Plasmas, 14, 012108, doi:10.1063/1.2435317, 2007.

Gosling, J. T., Asbridge, J. R., Bame, S. J., Paschmann, G., and Sckopke, N.: Observations of two distinct populations of bow shock ions in the upstream solar wind, Geophys. Res. Lett., 5, 957–960, 1978.

de Hoffmann, F. and Teller, E.: Magneto-Hydrodynamic Shocks, Phys. Rev., 80, 692–703, 1950.

Haaland, S. E., Sonnerup, B. U. Ö., Dunlop, M. W., Balogh, A., Georgescu, E., Hasegawa, H., Klecker, B., Paschmann, G., Puhl-Quinn, P., Rème, H., Vaith, H., and Vaivads, A.: Four-spacecraft determination of magnetopause orientation, motion and thickness: comparison with results from single-spacecraft methods, Ann. Geophys., 22, 1347–1365, 2004, http://www.ann-geophys.net/22/1347/2004/.

Hada, T., Oonishi, M., Lembège, B., and Savoini, P.: Shock front nonstationarity of supercritical perpendicular shocks, J. Geophys. Res., 108(A6), 1233, doi:10.1029/2002JA009339, 2003.

Harvey, C. C.: Spatial gradients and the volumetric tensor, in: Multi-Spacecraft Analysis, Chap. 12, ISSI, edited by: Paschmann, G. and Daly, P., 307–348, 1998.

Horbury, T. S., Cargill, P. J., Lucek, E. A., Eastwood, J., Balogh, A., Dunlop, M. W., Fornacon, K.-H., and Georgescu, E.: Four spacecraft measurements of the quasiperpendicular terrestrial bow shock: Orientation and motion, J. Geophys. Res., 107, 1208–1219, doi:10.1029/2001JA000273, 2002.

Kucharek, H., Möbius, E., Scholer, M., Mouikis, C., Kistler, L. M., Horbury, T., Balogh, A., Rème, H., and Bosqued, J. M.: On the origin of field-aligned beams at the quasi-perpendicular bow shock: multi-spacecraft observations by Cluster, Ann. Geophys., 22, 2301–2308, 2004, http://www.ann-geophys.net/22/2301/2004/.

Lin, R. P., Meng, C. I., and Anderson, K. A.: 30–100 keV protons upstream from the Earth bow shock, J. Geophys. Res., 79, 489–498, 1974.

Lembège, B. and Savoini, P.: Nonstationarity of a two-dimensional quasiperpendicular supercritical collisionless shock by self-reformation. Phys. Fluids, B, 4, 3533–3548, 1992.

Lobzin, V. V., Krasnoselskikh, V. V., Bosqued, J.-M., Pinçon, J.-M., and Schwartz, S. J.: Nonstationarity and reformation of high-Mach-number quasiperpendicular shocks: Cluster observations, Geophys. Res. Lett., 34, L05107, doi:10.1029/2006GL029095, 2007.

Lowe, R. E. and Burgess, D.: The properties and causes of rippling in quasi-perpendicular collisionless shock fronts, Ann. Geophys., 21, 671–679, 2003, http://www.ann-geophys.net/21/671/2003/.

Meziane, K., Wilber, M., Hamza, A. M., Mazelle, C., and Parks, G. K.: Evidence for a high-energy tail associated with foreshock field-aligned beams, J. Geophys. Res., 112, A01101, doi:10.1029/2006JA011751, 2007.

Moullard, O., Burgess, D., Horbury, T. S., and Lucek, E. A.: Ripples observed on the surface of the Earth's quasi-perpendicular bow shock, J. Geophys. Res., 111, A09113, doi:10.1029/2005JA011594, 2006.

Möbius, E., Kucharek, H., Mouikis, C., Georgescu, E., Kistler, L. M., Popecki, M. A., Scholer, M., Bosqued, J. M., Rème, H., Carlson, C. W., Klecker, B., Korth, A., Parks, G. K., Sauvaud, J. C., Balsiger, H., Bavassano-Cattaneo, M.-B., Dandouras, I., DiLellis, A. M., Eliasson, L., Formisano, V., Horbury, T., Lennartsson, W., Lundin, R., McCarthy, M., McFadden, J. P., and Paschmann, G.: Observations of the spatial and temporal structure of field-aligned beam and gyrating ring distributions at the quasi-perpendicular bow shock with Cluster CIS, Ann. Geophys., 19, 1411–1420, 2001, http://www.ann-geophys.net/19/1411/2001/.

Paschmann, G., Sckopke, N., Asbridge, J. R., Bame, S. J., and Gosling, J. T.: Energization of solar wind ions by reflection from the Earth's bow shock, J. Geophys. Res., 85, 4689–4693, 1980.

Rème, H., Aoustin, C., Bosqued, J. M., et al.: First multispacecraft ion measurements in and near the Earth's magnetosphere with the identical Cluster ion spectrometry (CIS) experiment, Ann. Geophys., 19, 1303–1354, 2001, http://www.ann-geophys.net/19/1303/2001/.

Russell, C. T., Mellott, M. M., Smith, E. J., and King, J. H.: Multiple spacecraft observations of interplanetary shocks Four spacecraft determination of shock normals, J. Geophys. Res., 88, 4739–4748, 1983.

Scholer, M., Shinohara, I., and Matsukiyo, S.: Quasi-perpendicular shocks: Length scale of the cross-shock potential, shock reformation, and implication for shock surfing, J. Geophys. Res., 108(A1), 1014, doi:10.1029/2002JA009515, 2003.

Schwartz, S. J., Thomsen, M. F., and Gosling, J. T.: Ions upstream of the Earth's bow shock – A theoretical comparison of alternative source populations, J. Geophys. Res., 88, 2039–2047, 1983.

Schwartz, S. J. and Burgess, D.: On the theoretical/observational comparison of field-aligned ion beams in the Earth's foreshock, J. Geophys. Res., 89, 2381–2384, 1984.

Schwartz, S. J.: Shock and discontinuity normals, mach numbers, and related parameters, in: Multi-Spacecraft Analysis, Chap. 10, ISSI, edited by: Paschmann, G. and Daly, P., 249–270, 1998.

Sonnerup, B. U. Ö.: Acceleration of particles reflected at a shock front, J. Geophys. Res., 74, 1301–1304, 1969.